CHAPTER 3

RESULTS AND DISCUSSION

3.1 POWDERS CHARACTERIZATION

PZT and PLZT powders synthesized from hydrothermal process were characterized by the following methods.

3.1.1 INVESTIGATION OF THERMAL DECOMPOSITION

3.1.1.1 PZT Powders from Hydrothermal Process

The TGA-DTA curves of the intermediate PZT hydrothermal product are shown in Figure 3.1. This picture shows two endothermic peaks associated with two TGA weight loss regions at about 80 °C and 930 °C. Between 300 °C and 900 °C the weight loss was stable. The first weight loss was attributed to the desorption of surface adsorbed hydroxyl group, which possessed various bonding energies with the surface owing to their adsorption on several surface sites with different coordination numbers and mostly desorbing at about 100 °C[111]. The second small endothermic peak at around 350 °C was due to the decomposition of organic groups, mainly acetate and propoxide groups bonded to the zirconium and titanium atoms. The last endothermic peak occurred around 900 to 1000 °C was attribted to the evaporation of PbO in PZT powders.[110] The overall weight loss was 3.20 percent.

Figure 3.2 shows thermogravimetric analysis and differential thermal analysis of PLZT powders synthesized by the hydrothermal process. The TGA and DTA curves exhibited the same results as Figure 3.1. The overall weight loss was 4.67 percent.

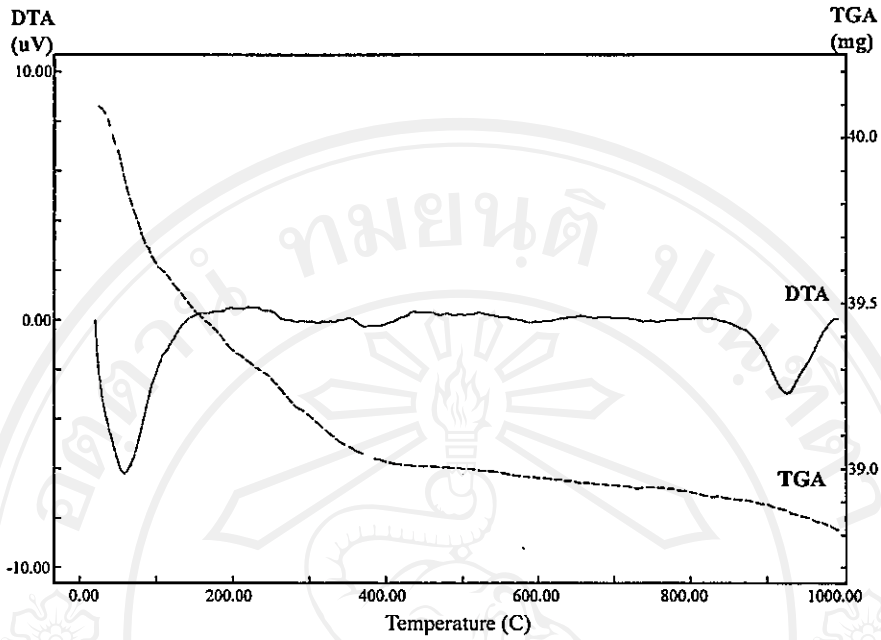

Figure 3.1 Thermogravimetric and differential thermal analysis of PZT powders synthesized by hydrothermal process.

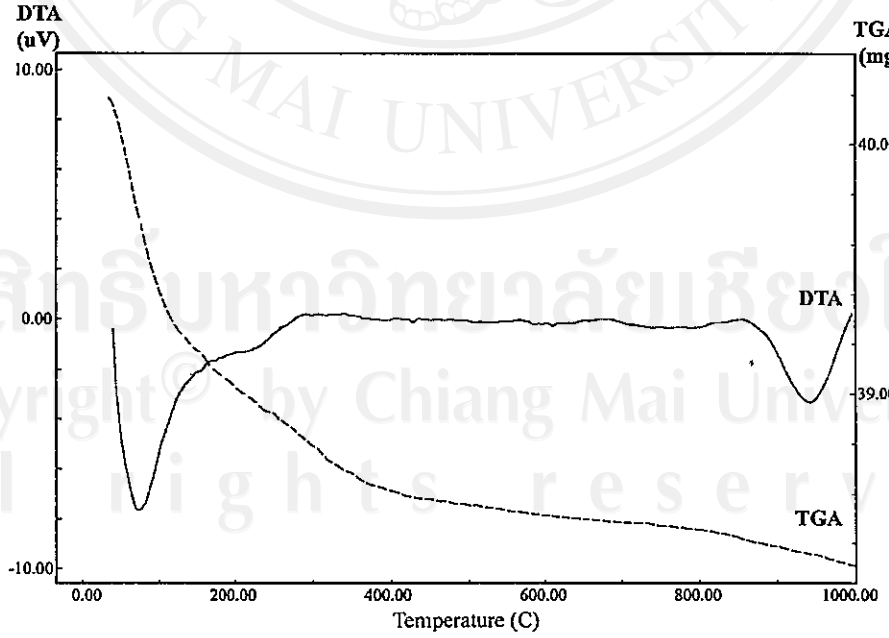

Figure 3.2 Thermogravimetric and differential thermal analysis of PLZT powders synthesized by hydrothermal process.

3.1.2 CRYSTALLINE STRUCTURE DETERMINATION

3.1.2.1 PZT Powders from Hydrothermal Process

3.1.2.1.1 Effect of Mineralizer Concentration

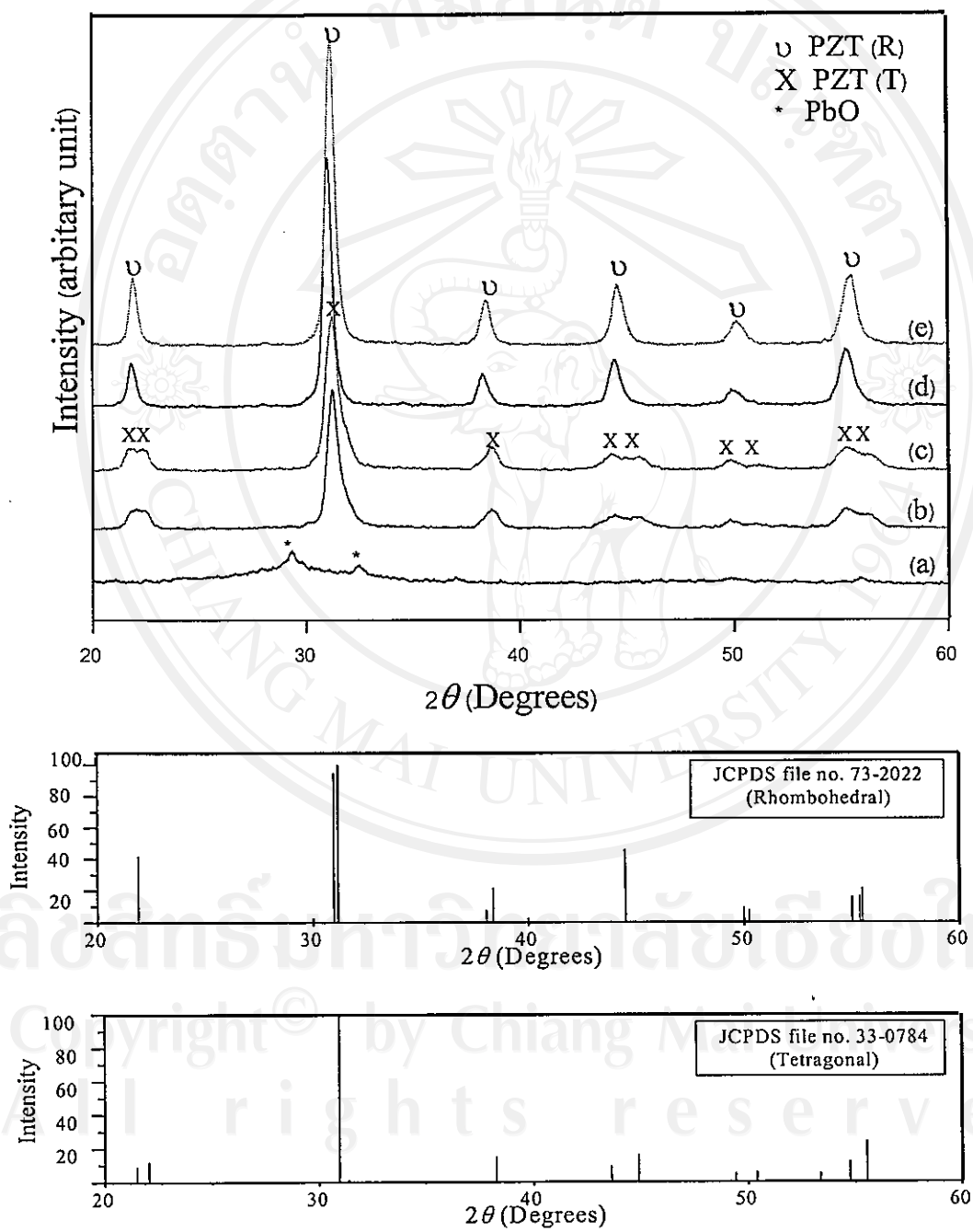

Figure 3.3 XRD patterns of PZT powders synthesized by hydrothermal process at different KOH concentrations as (a) 1.0 M KOH, (b) 2.0 M KOH, (c) 3.0 M KOH, (d) 4.0 M KOH and (e) 5.0 M KOH

The effect of mineralizer concentration on hydrothermally synthesized PZT powders is given in Figure 3.3. The synthesis time was fixed at 6 hours while the synthesis temperature was 200 °C. At low KOH concentration (1.0 M KOH), the product was amorphous and some PbO peaks occurred. At higher KOH concentration, phase pure perovskite PZT was formed. At 2.0 M and 3.0 M KOH, perovskite PZT had a tetragonal structure as shown from the peak splitting around $2\theta \sim 45$ degrees in XRD patterns (JCPDS file number 33-0784). At relatively high concentration (4.0 M and 5.0 M KOH), tetragonal perovskite PZT were transformed to the rhombohedral form. The results indicated that the PZT composition shifted to the $PbZrO_3$ rich side of the PZT phase diagram (Figure 1.6) as the concentration of KOH increased.

3.1.2.1.2 Effect of pH Value

The effect of pH values on hydrothermally synthesized PZT powders is illustrated in Figure 3.4. The synthesis time was fixed at 6 hours while the synthesis temperature was 200 °C. 4.0 M KOH was used as mineralizer to various pH values (pH value varied from 10 to 14). At low pH value (at pH 10), the product was amorphous. And at relalive high pH values (pH 11 and 12), the products were composed of PbO and TiO_2. Perovskite phase PZT was formed at higher pH values. The critical pH value required for perovskite PZT formation was 13. At pH 13 and 14, perovskite phase PZT was formed completely. Rhombohedral phase occurred as the major phase in the XRD patterns.

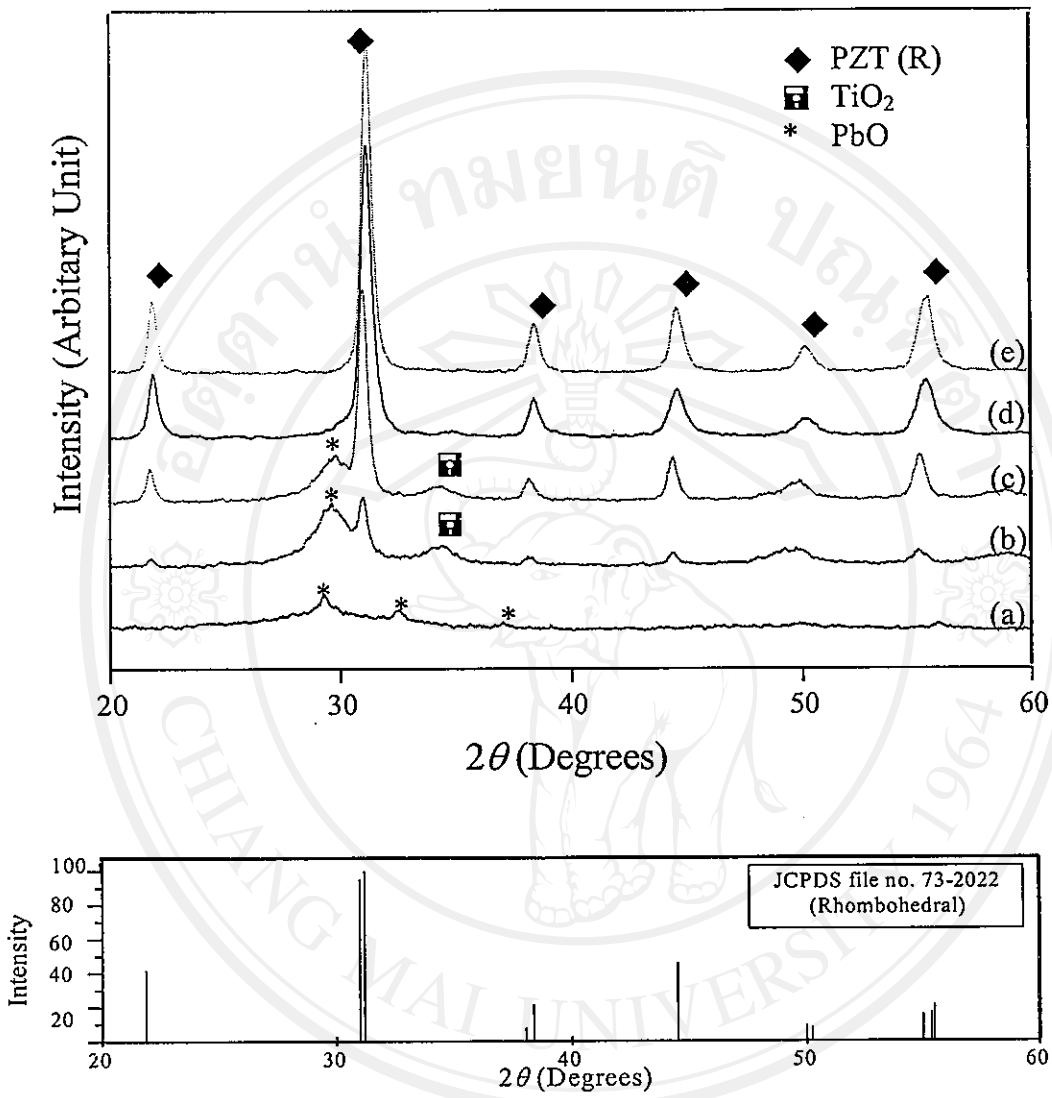

Figure 3.4 XRD patterns of PZT powders synthesized by hydrothermal process using KOH as a mineralizer at different pH values as (a) pH 10, (b) pH 11, (c) pH 12, (d) pH 13 and (e) pH 14

3.1.2.1.3 Effect of Holding Period

The effect of holding period on perovskite PZT formation is shown in Figure 3.5. The synthesis temperature was fixed at 200 °C and 4.0 M KOH was used as a mineralizer. The holding period was varied from 2 to 48 hours. At 2 and 4 hours,

the XRD patterns showed no obvious signs of perovskite PZT, the products were amorphous and composed of TiO_2 and PbO. Above 6 hours, phase pure perovskite rhombohedral PZT was formed. It can be seen clearly from the XRD patterns that the critical holding period for PZT powders by hydrothermal process at this condition was 6 hours. Rhombohedral PZT was formed at the holding period of 6 hours and longer.

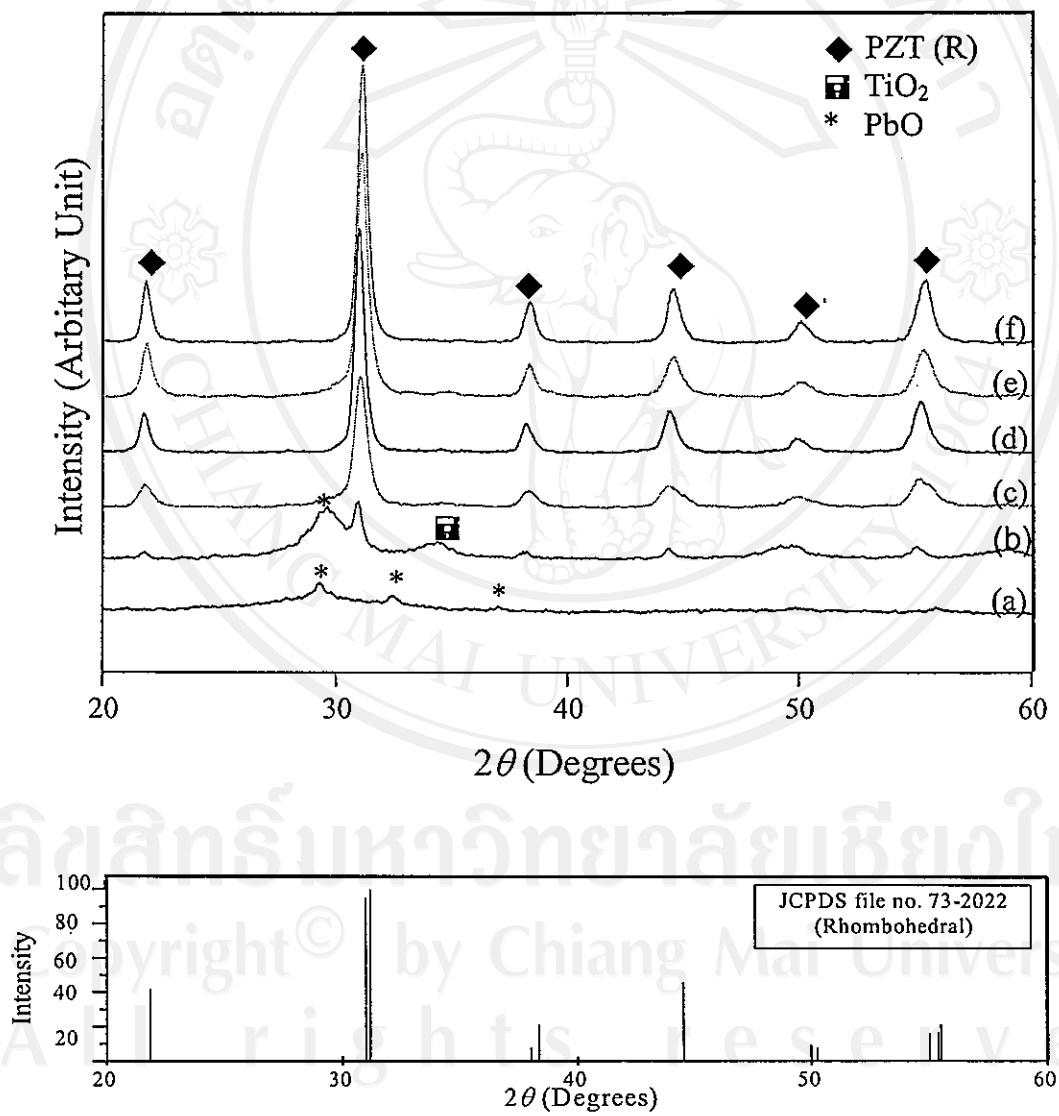

Figure 3.5 XRD patterns of PZT powders synthesized by hydrothermal process at 200 °C using 4.0 M KOH at pH =14 as a mineralizer at different synthesis times as (a) 2 h, (b) 4 h, (c) 6 h, (d) 12 h, (e) 24 h and (f) 48 h

3.1.2.4 PLZT Powders from Hydrothermal Process

The XRD pattern of PLZT powders at the different mole %La synthesized by the hydrothermal process at 200 °C for 6 hours using 4.0 M KOH at pH 14 as a mineralizer is given in Figure 3.6. From XRD patterns, a cubic phase of PLZT occurred and matched with the JCPDS file number 46-0336. The desired PLZT compositions was 0.88:0.12: 0.52:0.48 for 12mol% PLZT.

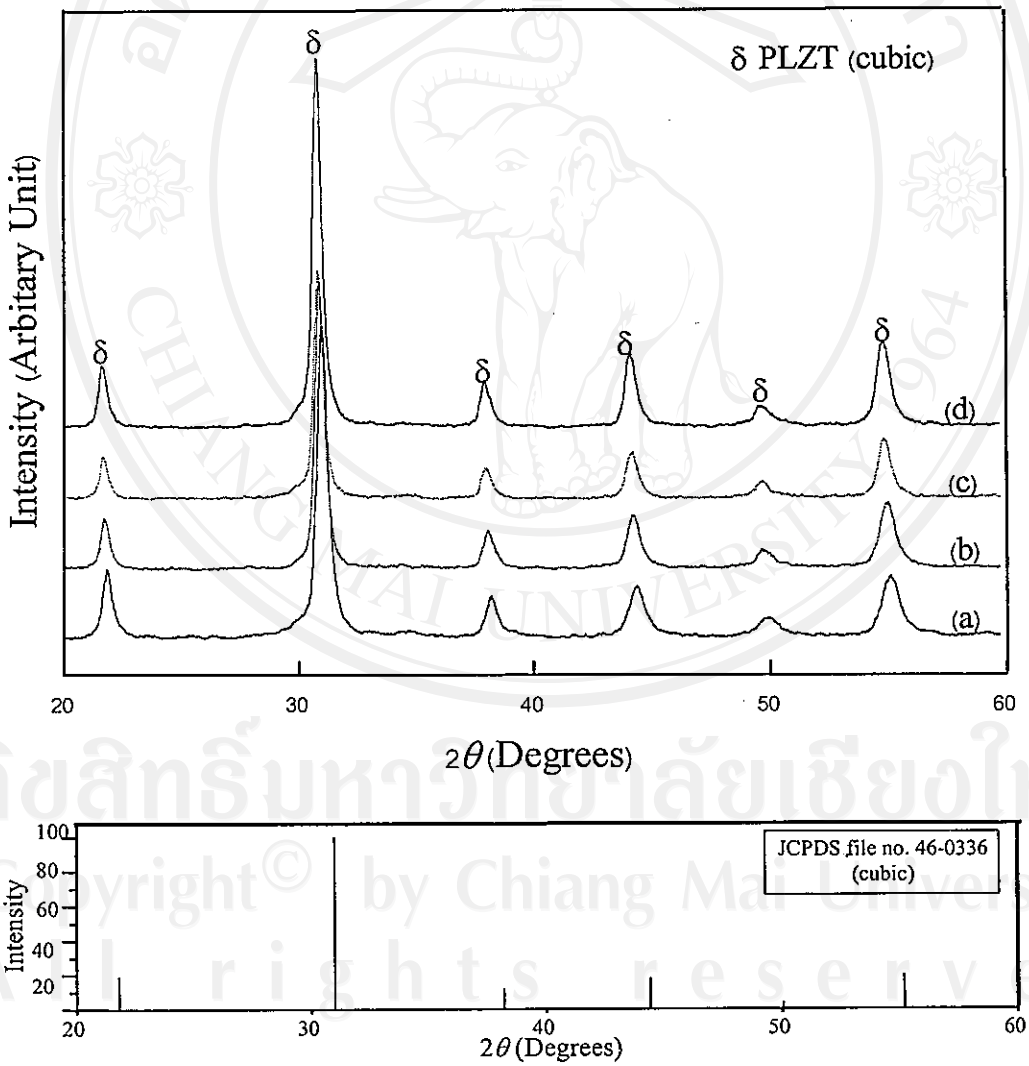

Figure 3.6 XRD patterns of PLZT powders synthesized by hydrothermal process at 200 °C for 6 hours using 4.0 M KOH as a mineralizer in different mole% La at (a) 8 %La, (b) 9 %La, (c) 10 %La and (d) 12 %La.

The effect of lanthanum doped in PZT are interesting because of the substitution of Pb^{2+} ion by La^{3+} ion creates vacancies in the A-site and also, can create vacancies in the B-site of the perovskite ABO_3 structure PZT ceramic. The long-rang interaction between ferroelectrically active oxygen octahedral interaction contain B-sites cations can break by incorporation of La^{3+} ions and vacancies in the lattice. Once a vacancy has been created, further motion of atoms is relatively easy by a neighboring atom hopping into the vacancy, which leads to vacancy migration. PLZT ceramics with a 12% La^{3+} concentration, being in the vicinity of the morphotropic phase boundary (MPB), have been reported to be a good quadratic modulator material. The PLZT ceramics with 12 mol% La^{3+} was reported to be used as pyroelectric material. The detailed studies of structural and electrical properties of the sample have been done to investigate the nature of PLZT in this composition.

3.1.3 MICROSTRUCTURE ANALYSIS

3.1.3.1 PZT Powders from Hydrothermal Process.

3.1.3.1.1 Effect of Mineralizer Concentration

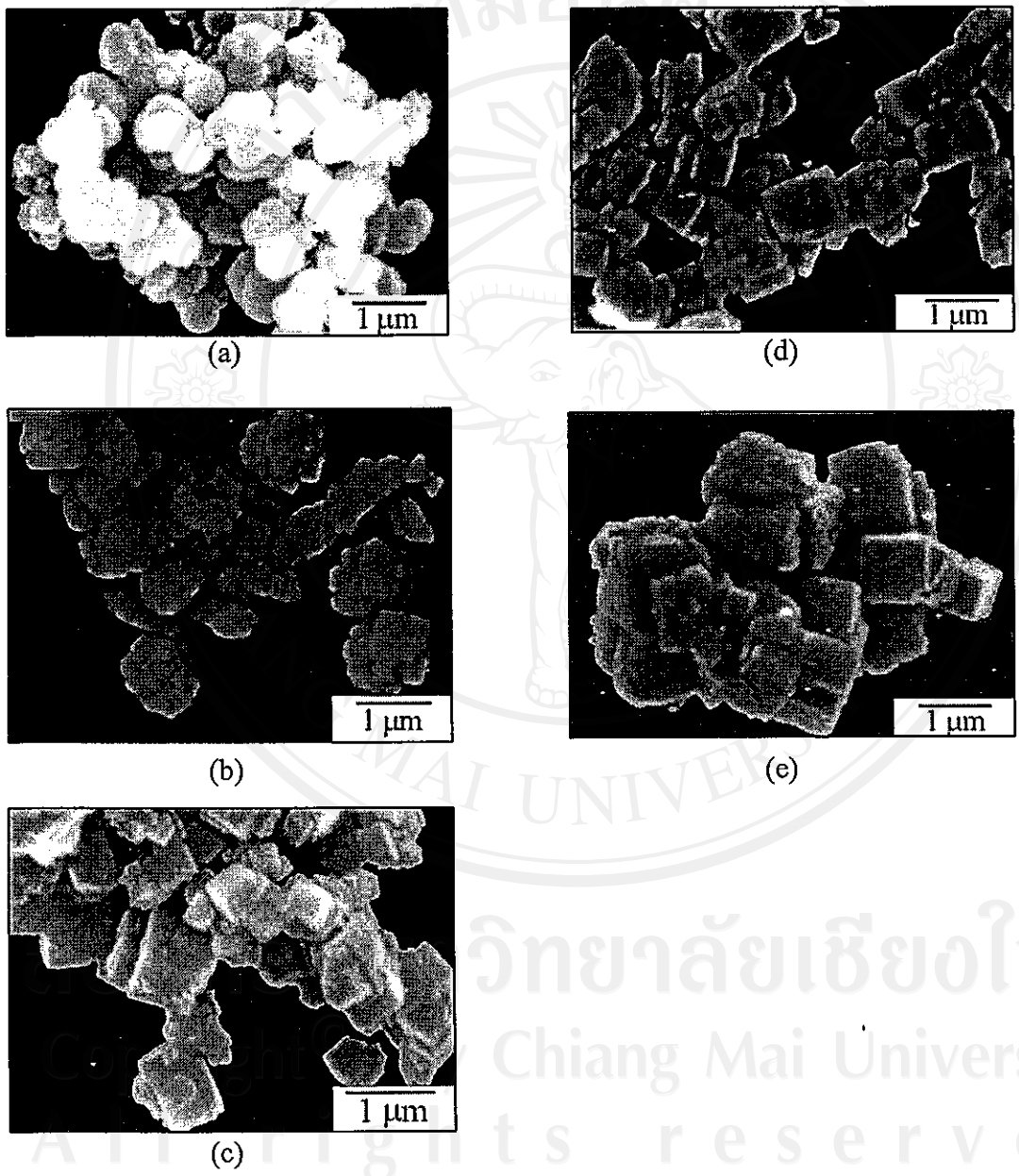

Figure 3.7 SEM micrographs of PZT powders obtained from hydrothermal process at 200 °C for 6 hours using KOH at as a mineralizer in different concentrations as (a) 1.0 M, (b) 2.0 M, (c) 3.0 M, (d) 4.0 M and (e) 5.0 M KOH.

Figure 3.7 [(a)-(e)] shows SEM micrographs of PZT powders synthesized by hydrothermal process at 200 °C for 6 hours using KOH as a mineralizer in different molar concentrations. As the KOH concentration increased, the particle size and the agglomeration increased significantly. At 1.0 and 2.0 M KOH, the powders showed pseudocubic forms. At higher molar concentrations (4.0 and 5.0 M KOH), the powders morphology transformed to the cubic particles. The particle size increased from 0.3 - 0.7 μm, (Figure 3.7 (d)), to about 0.75 μm, (Figure 3.7 (e)), when the KOH concentration increased from 4.0 to 5.0 M.

3.1.3.1.2 Effect of pH Value

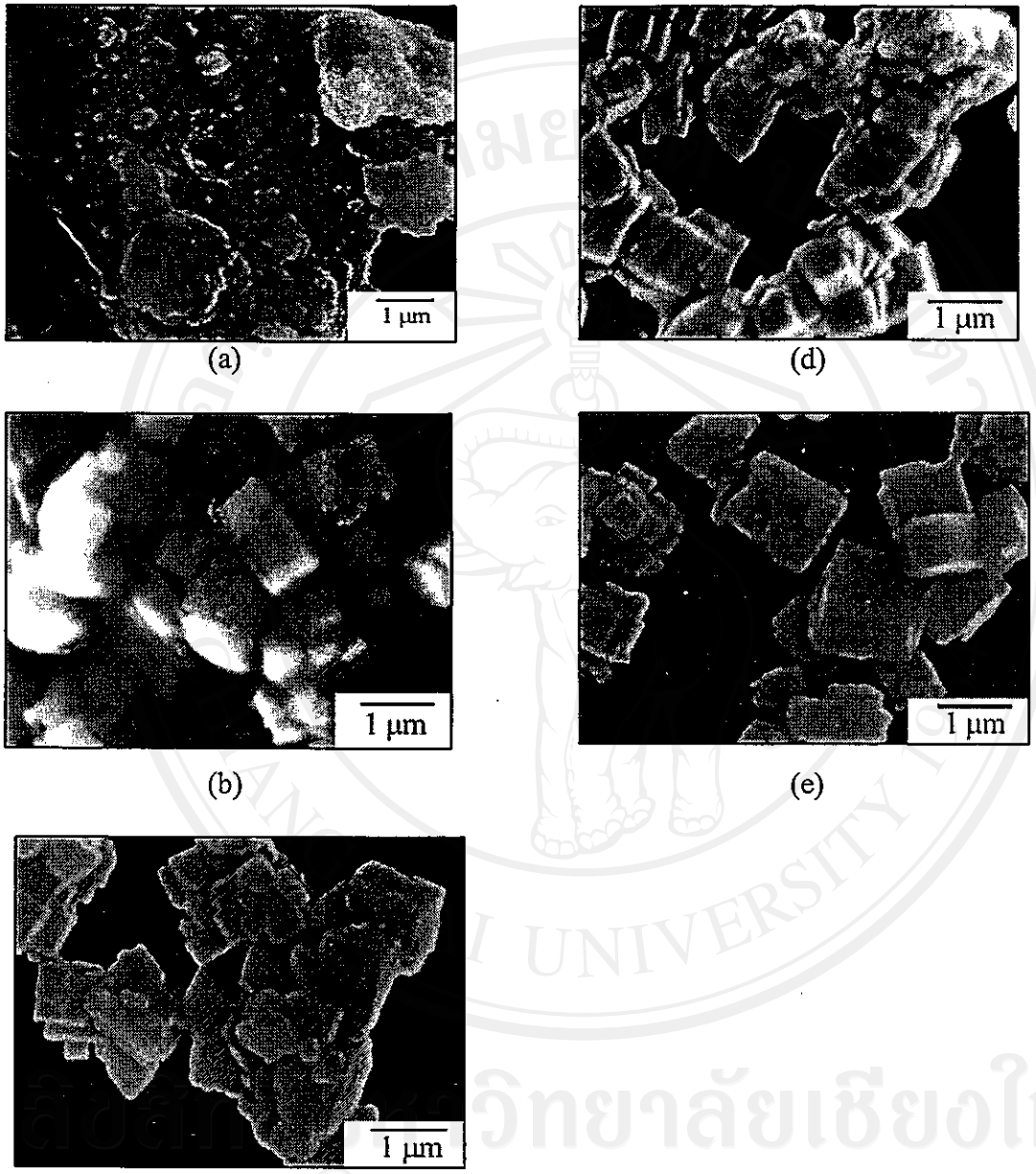

Figure 3.8 SEM micrographs of PZT powders obtained from hydrothermal process at 200 °C for 6 hours using 4.0 M KOH as a mineralizer in different pH values as (a) pH 10, (b) pH 11, (c) pH 12, (d) pH 13 and (e) pH 14

Figure 3.8 [(a)-(e)] shows SEM micrographs of PZT powders synthesized by hydrothermal process at 200 °C for 6 hours using 4.0 M KOH as a mineralizer at different pH values. At low pH value, pH 10 (Figure 3.8(a)), the powders were amorphous and irregular in shape. At pH 11 and 12 [Figure 3.8 (b) and (c)], the products were not completely crystallite and the powder's morphology became the cubic particles. At higher pH value, pH 13 and 14, it can be seen clearly from Figure 3.8 (d) and (e) that the powders were the cubic particles and their sizes ranged between 0.5 μm to 1.0 μm

3.1.3.1.3 Effect of Synthesis Time

SEM micrographs of PZT powders synthesized by hydrothermal process at 200 °C using 4.0 M KOH at pH 14 as a mineralizer at different synthesis time from 2 to 48 hours are illustrated in Figure 3.9 [(a)-(f)]. As the synthesis time increased, both the particle size and the extent of particle agglomeration increased. After synthesis time of 2 and 4 hours, Figure 3.9 (a) and (b), the morphology became more cubic with an increased size of 0.25 μm to 0.33 μm. At the synthesis time of 6 hours and longer, Figure 3.9 (c) to (f), the cubic morphology was fully developed, the particle sizes increased to between 0.33 μm and 1.0 μm but the size distribution of the longer synthesis time was narrower than the shorter synthesis time.

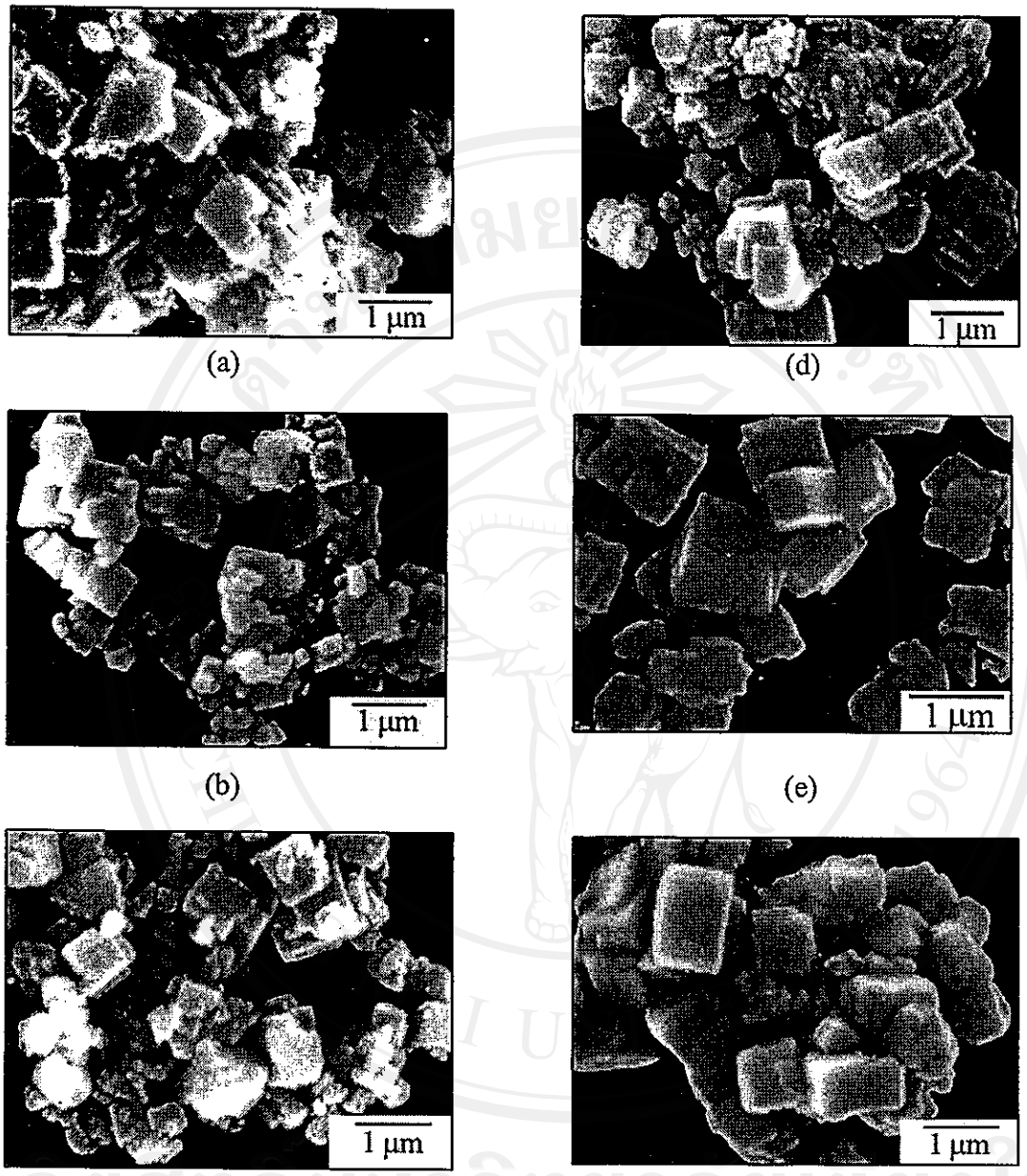

Figure 3.9 SEM micrographs of PZT powders obtained from hydrothermal process at 200 °C using 4.0 M KOH at pH 14 as a mineralizer at different holding periods as (a) 2 h, (b) 4 h, (c) 6 h, (d) 12 h, (e) 24 h and (f) 48 h.

3.1.3.2 PLZT Powders from Hydrothermal Process

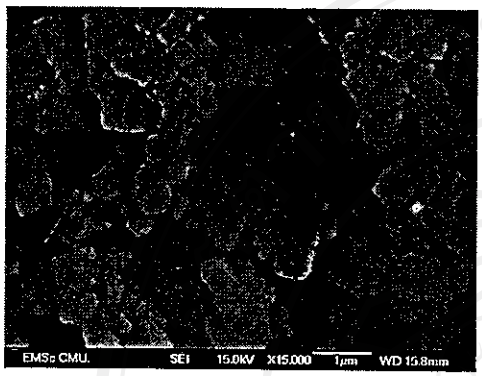

(a)

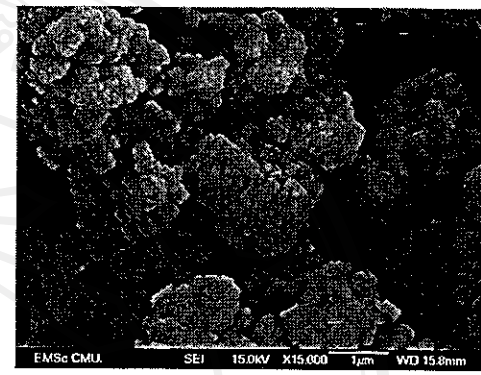

(b)

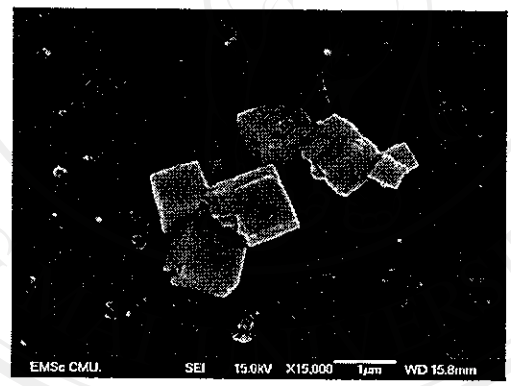

(C)

Figure 3.10 SEM micrograph of PLZT powders at 12 %La synthesized by hydrothermal process at 200 °C for (a) 8 hours (b) 12 hours (c) 24 hours using 4.0 M KOH at pH 14 as a mineralizer.

Figure 3.10 shows SEM micrograph of PLZT powders containing 12 mole % La obtained through hydrothermal process at 200 °C for 8, 12 and 24 hours using 4.0 M KOH as a mineralizer. As can be seen from this micrograph, PLZT powders showed well-developed crystallite products, which had cubic shape with some agglomeration occurring between the cubic particles. As the holding periods step up gradually with holding from 8, 12 and 24 hours, the resulting particle size ranges from 0.2-0.3 μm, 0.2-0.3 and 0.3-1.0 μm, respectively.

3.2 CERAMICS CHARACTERIZATION

3.2.1 Densification of PZT ceramics

The PZT powders from the hydrothermal process, at a synthesis temperature of 200 °C for 6 hours using 4.0 M KOH as a mineralizer, was selected for densification measurements because of their similar rhombohedral structure. PZT powders were pressed and sintered at temperature from 1000 °C to 1250 °C for 3 and 5 hours. Their results are illustrated in Table 3.1.

The theoretical density of the rhombohedral PZT, estimated from the lattice parameters, was 8.085 g/cm^3, while the theoretical density of the tetragonal PZT was 8.006 g/cm^3, The average theoretical density used for calculations (%theoretical density) was 8.045 g/cm^3. The sintered pellet density was measured by an immersion technique and calculated from Archimedes' principle.

From Table 3.1, the suitable sintering temperature for PZT ceramics obtained from the coprecipitation process was 1150 °C for 5 hours because at lower sintering temperatures and times the ceramics were less dense, while at higher sintering temperatures and times, there density was not change. For PZT ceramics obtained

from the hydrothermal process, suitable sintering temperature was 1250 °C for 5 hours.

Table 3.1 The measured density, % theoretical density, and % linear shrinkage of PZT powders obtained from hydrothermal process.

Sintering temperature (°C)	Sintering time (h)	Measured density (g/cm^3)	Theoretical density (%)	Linear shrinkage (%)
1000	3	5.54	68.85	9.12
1100	3	6.02	74.82	11.07
1150	3	6.58	81.78	12.97
1200	3	7.32	90.99	13.25
1250	3	7.44	92.47	13.48
1000	5	5.67	70.47	9.99
1100	5	6.14	76.31	11.55
1150	5	6.69	83.15	13.01
1200	5	7.43	92.35	13.32
1250	5	7.62	94.71	13.5

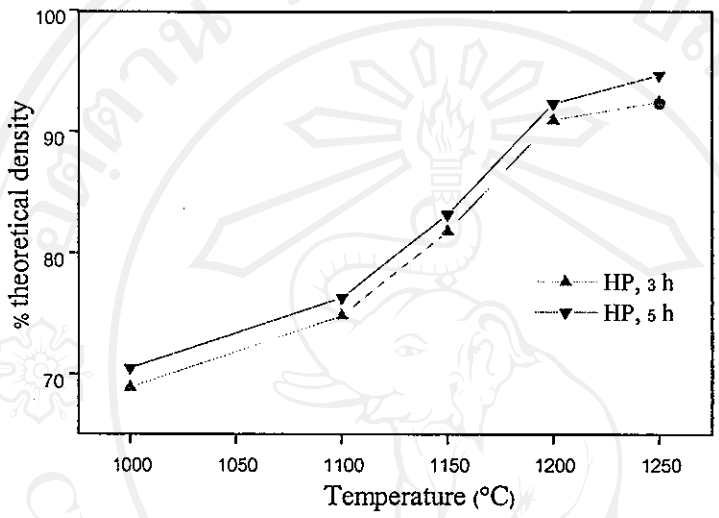

Figure 3.11 Percent theoretical density versus sintering temperature curves at sintering time of 3 and 5 hours.

Percent theoretical density versus sintering temperature curves at sintering time of 3 and 5 hours are shown in Figure 3.11. The sintered density of PZT increased rapidly until a temperature of 1200 °C then increased slightly with increasing sintering temperature and reached the maximum at temperature of 1250 °C.

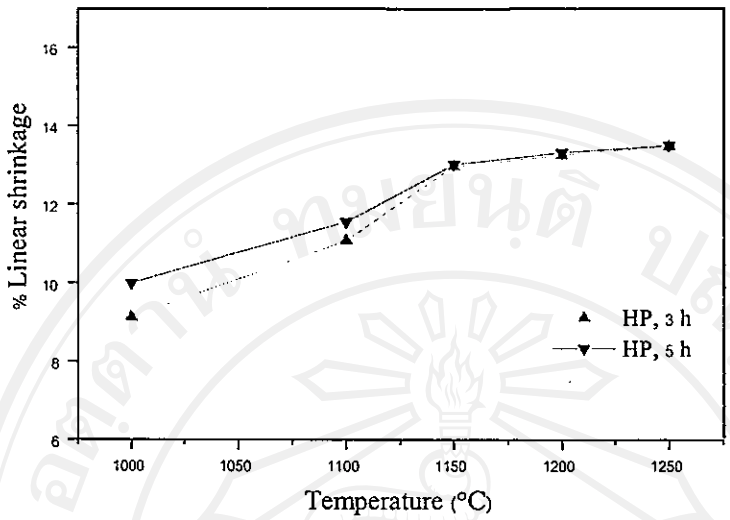

Figure 3.12 Percent linear shrinkage versus sintering temperature at sintering time of 3 and 5 hours .

Percent linear shrinkage versus sintering temperature curves at sintering time of 3 and 5 hours are given in Figure 3.12. The shrinkage in PZT ceramics has a close relationship with the weight losses (see Figure 3.1 and 3.3). And weight loss during sintering mainly occurred from the evaporation of lead oxide.

3.2.2 XRD patterns of PZT and PLZT Ceramics

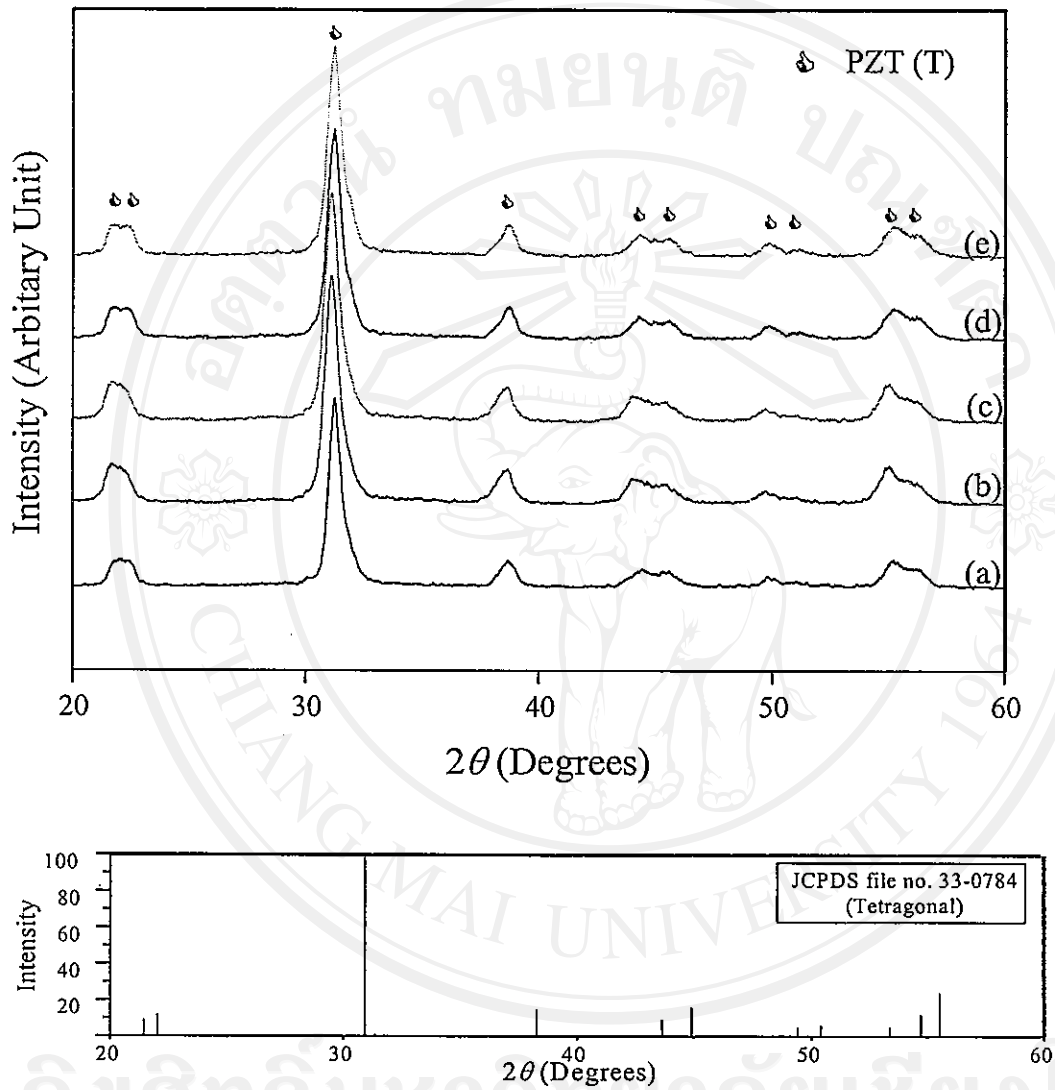

Figure 3.13 XRD patterns of sintered PZT ceramics obtained from hydrothermal process for 5 hours at different sintering temperatures at (a) 1000 °C, (b) 1100 °C, (c) 1150 °C, (d) 1200 °C and (e) 1250 °C

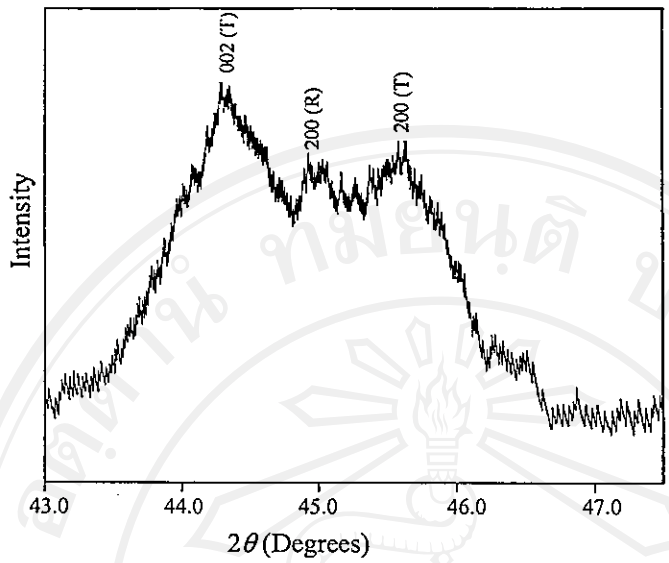

Figure 3.14 Fine structure in XRD pattern of PZT ceramics obtained from hydrothermal process sintered at 1250 °C at 2θ from 43 to 47 degrees

XRD patterns of hydrothermally synthesized PZT at different sintering temperatures are given in Figures 3.13 and 3.14. XRD patterns indicated that, as sintering temperature increased, the peaks at 2θ nearly 45 degree splitted into three peaks of 200 (T), 002 (T) and 200 (R) for the coexisted phases between tetragonal and rhombohedral structures[121, 122]. This split peak did not occur in the initial hydrothermally synthesized PZT powders. The change in the crystal structure of PZT ceramics from rhombohedral to tetragonal was due to the loss of lead oxide which also resulted in the precipitation of ZrO_2. This moved the compositions from MPB towards the ZrO_2 - PZT region[120]. However the ZrO_2 reflection was not shown in the XRD results, probably because of its content was below the XRD detection limit or its crystal size was too small (< 10 nm).

These results could confirm by thermogravimetric analysis of PZT powders (Figure 3.1 and 3.3). The thermal decomposition of hydrothermally synthesized PZT lost its second weight at about 900 °C.

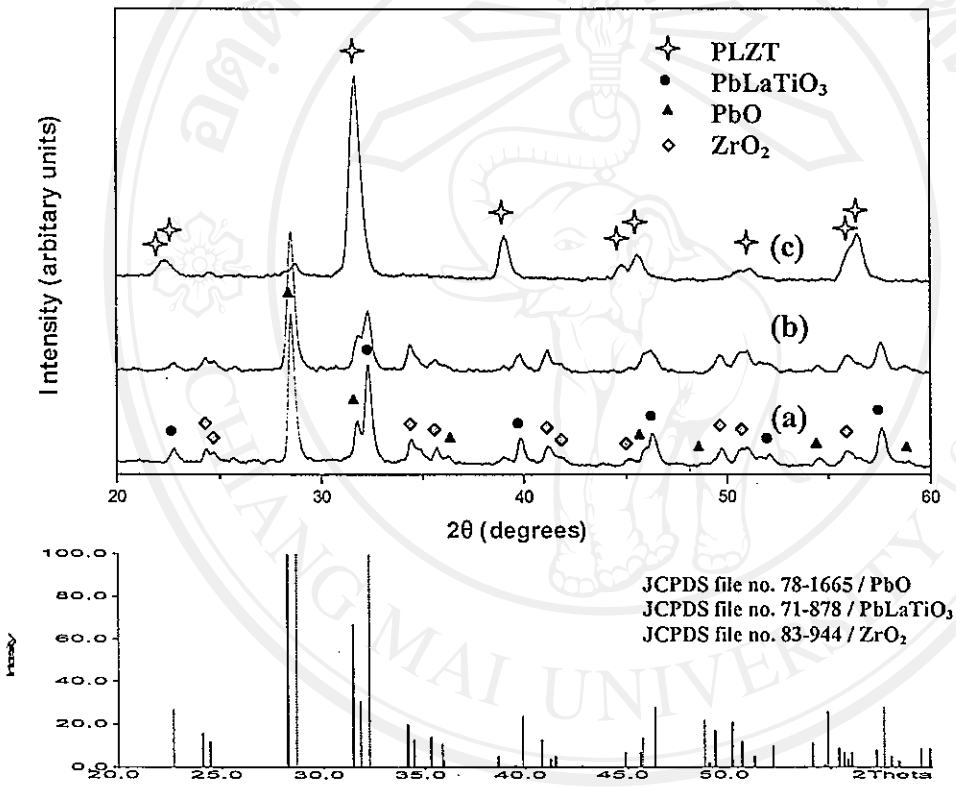

Figure 3.15. XRD patterns of PLZT ceramics sintered at 1300 ^{0}C for 3 h prepared from powders with different holding periods of (a) 8 h (b) 12 h and (c) 24 h

Figure 3.15 shows the XRD patterns for ceramics prepared from powders for different reaction times. A tetragonal perovskite-type structure was identified for ceramics prepared from powders for a reaction time of 24 hours but also showed small amounts of PbO (e.g. peak at $2\theta = 28.7^{0}$). Ceramics prepared from PLZT powders for reaction times of 8 h and 12h contain some PbO, $PbLaTiO_3$ and ZrO_2 as indicated in Figure 3.15.

3.2.3 Microstructure of PZT and PLZT ceramics

The microstructure and grain size of the sintered samples were studied using scanning electron microscopic. Figure 3.16 shows SEM micrographs of PZT ceramics obtained from hydrothermal process sintered at 1150 °C to 1250 °C for 5 hours. At 1150 °C, Figure 3.16 (a), the microstructure exhibited some porous structure. At 1200 °C, Figure 3.16 (b), the microstructure exhibited bigger grain size with smaller pores than the PZT sintered at 1150 °C. The grain sizes increased to 1.0 μm - 1.5 μm. Finally, when the sintering temperature was raised to 1250 °C, the density increased to 94.71 % and the grain sizes were in the range of 3 μm to 5 μm

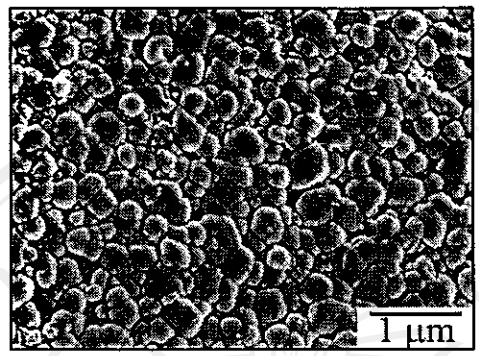

(a)

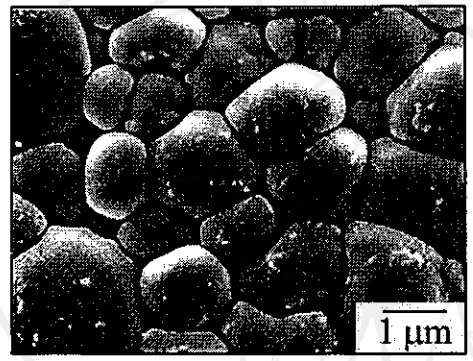

(b)

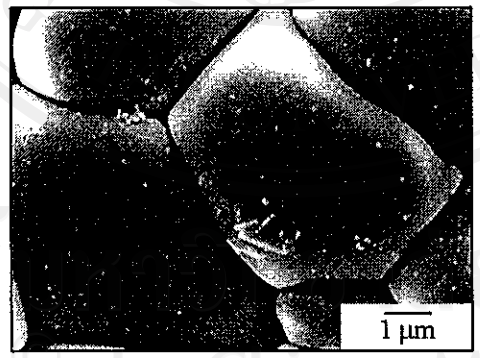

(c)

Figure 3.16 SEM micrographs of PZT ceramics obtained from hydrothermal process sintered for 5 hours at (a) 1150 °C, (b) 1200 °C and (C) 1250 °C

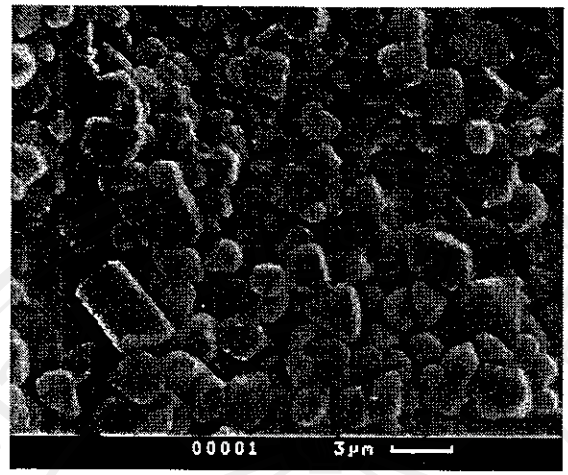

(a)

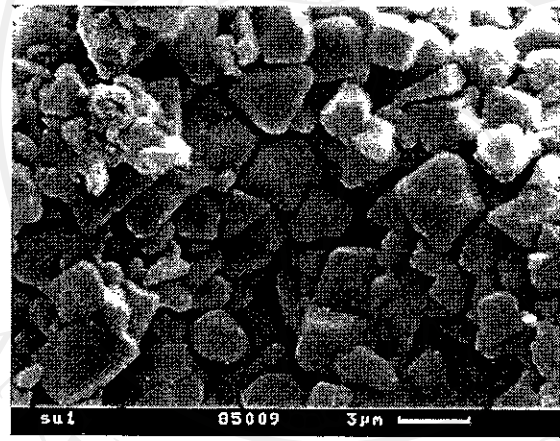

(b)

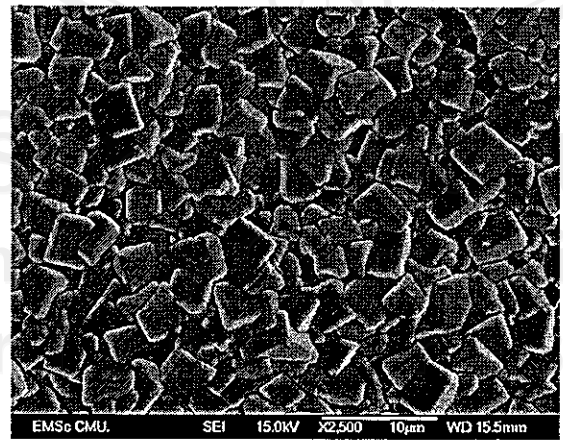

(c)

Figure 3.17. SEM micrographs of PLZT ceramics obtained from hydrothermal process sintered for 5 hours at (a) 1100 °C, (b) 1200 °C and (C) 1300 °C

The SEM micrographs of the fracture surfaces with various sintering temperatures are shown in figure 3.17. With higher sintering temperatures of 1100 ^{0}C, 1200^{0}C and 1300 ^{0}C, the microstructure consists of randomly oriented grain tightly bonded together, with averaged grain sizes of 2.8μm, 3.1μm and 4.3μm respectively. The small grain size was affected by small initial particle size. We can observe that the microstructure of sintered PLZT was not homogeneous. It's corresponding to the result of XRD in figure 3.15. These results can be approved by the formation of oxygen vacancies by evaporating PbO. The evaporation of PbO generates lattice vacancies near the surface as follows:

$Pb_{Pb} + O_o = V''_{Pb} + V_O^{\cdot\cdot} + PbO_{(g)}$

Therefore, the densification always initiates from the surface and proceeds into the body of material with sintering time and temperature.

3.2.4 Dielectric Properties

3.2.4.1 Impedance spectra of PZT and PLZT ceramics.

Figures 3.18 and 3.19 show the impedance spectra of PZT and PLZT ceramic at different measuring temperatures. At elevated temperature, only a well-formed arc is observed, implying one component is responsible for the conductive mechanism in samples (Figure 3.18). Since the complex impedance reaches zero when the measuring signal frequency (f) tend to ∞, the bulk materials or grain can be defined in the equivalent circuit composed by a grain resistance (R_G) and grain capacitance (C_G). However, in figure 3.19, two semicircle are easily resolved: one at high frequencies due to the contribution of ceramics grain to the electrical resistivity and the other due

to the contribution of grain boundary to the electrical resistivity. By comparing figure 3.18 and 3.19, it is evident that the conductive mechanism of PZT ceramic at high temperature is greatly changed with a Lanthanum addition.

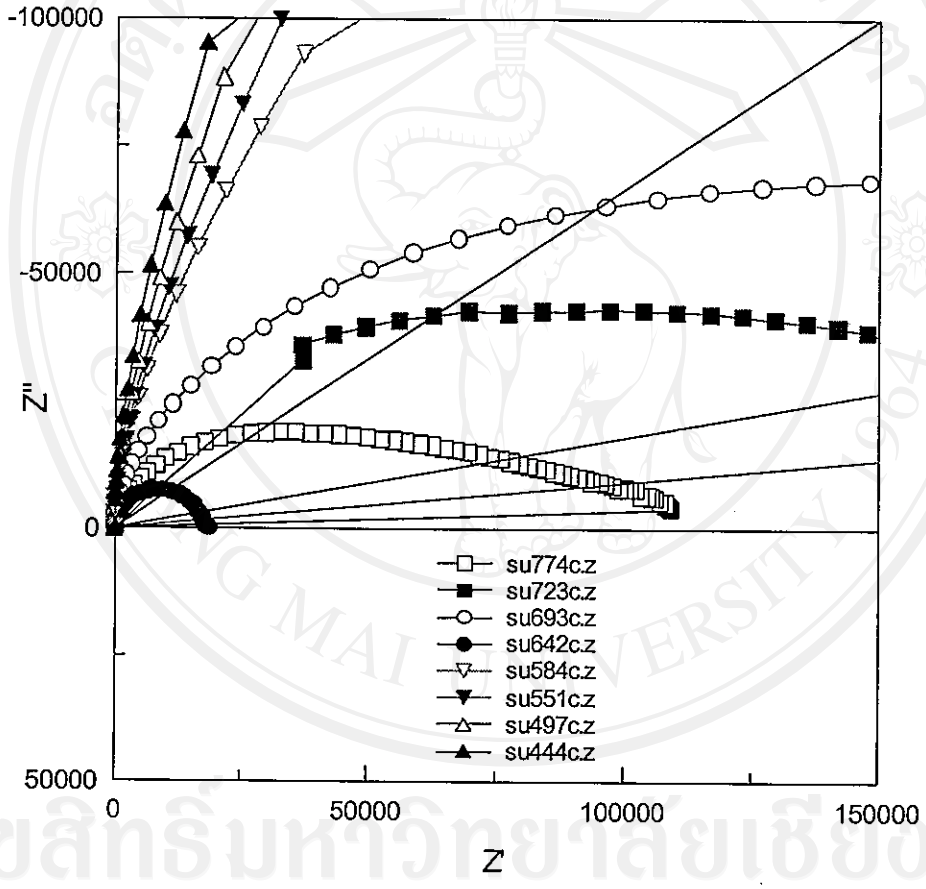

Figure 3.18 The complex impedance plot of PZT measured at 350 to 650 ^{o}C with increasing 50 ^{o}C by step.

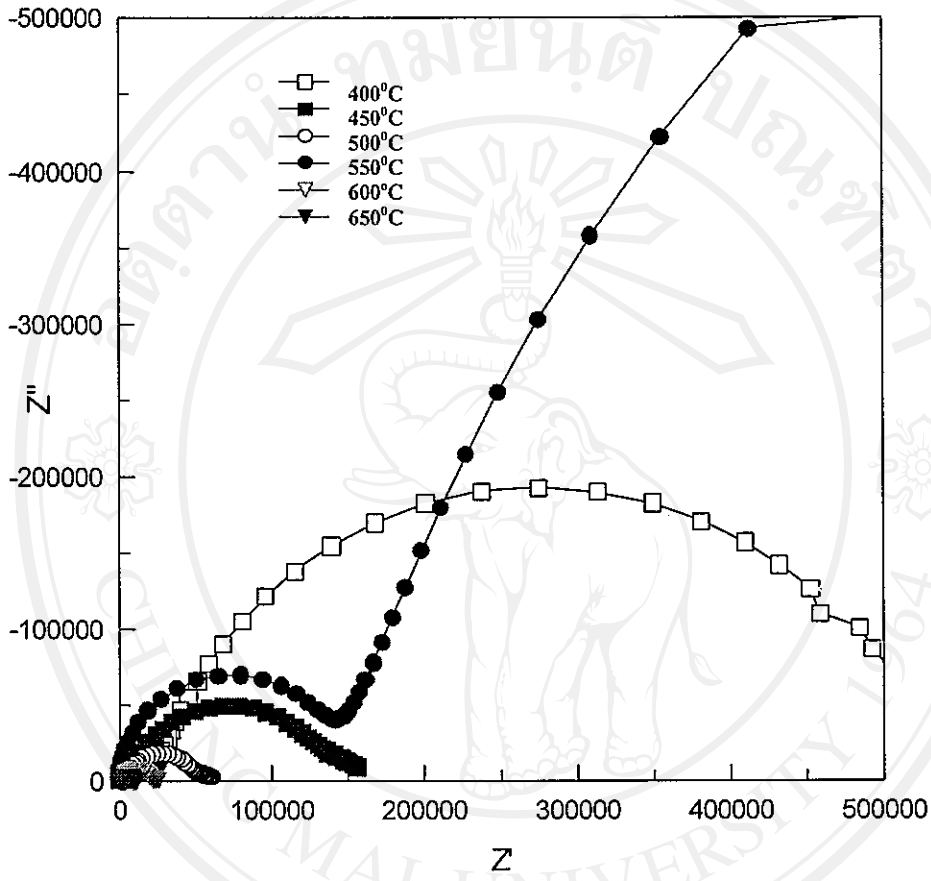

Figure 3.19 The complex impedance plot of PLZT measured at 400 to 650 ^{O}C with increasing 50 ^{O}C by step.

Figure 3.19 shows the impedance spectra of PLZT ceramics at different measuring temperatures(350- 650). Two semicircles are easily resolved: one at high frequencies (right intersect) is ascribed to total resistance (R_T), while the intersection at low frequency (left intersect) stands for grain resistance (R_G). The grain boundary resistance($R_{G.B.}$) value is then given as $R_{G.B.}= R_T-R_G$. The precise value of each component (R_G and $R_{G.B.}$) can be estimated from fitting of experimental data as in figure 3.20(a) and (b).

Figures 3.20(a) and (b) which show the experimental data taken at 400°C as well as simulated curves and the equivalent circuit employed.

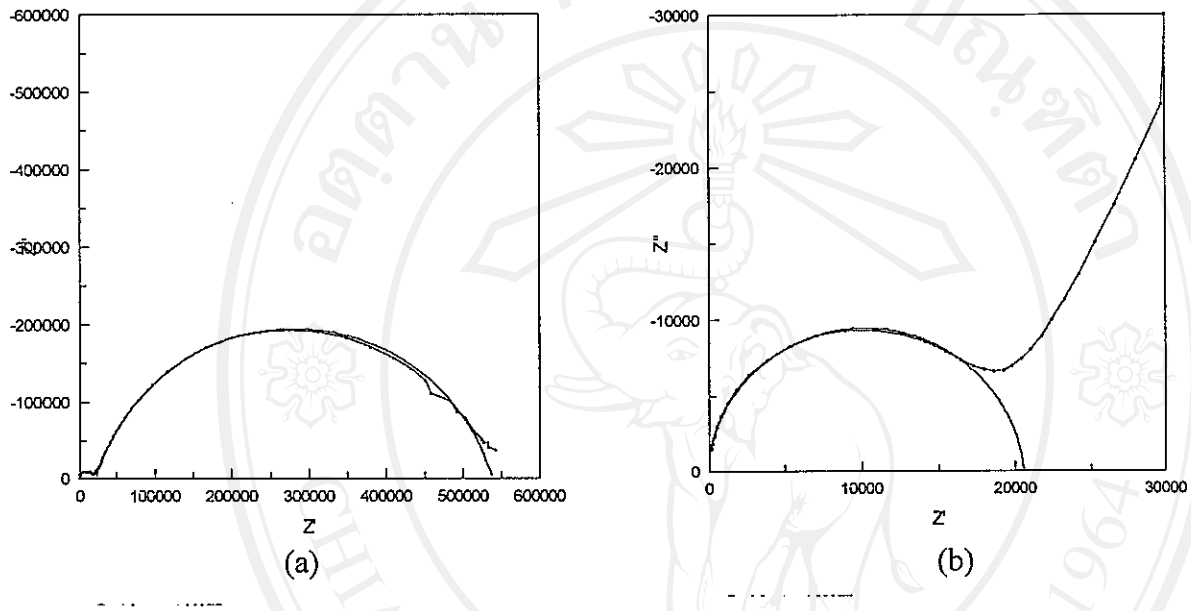

Figure 3.20 (a) A complex impedance plot of PLZT at 400 ^{O}C
(b) The simulated curve fitted to an equivalent to simple parallel circuit

From the result of impedance spectroscopy as in Figure 3.19, The log(R) and 1/T were calculated and processed Arrhenius dependence plot of PLZT ceramic as shown in Figure 3.21. The Arrhenious diagram in Figure 3.21 show two linear regions with different slope for R_G and $R_{G.B.}$. The activation energy (E_a) of R_G and $R_{G.B.}$ was calculated to be 1.1 and 1.8 eV, respectively, in terms of the slopes of fitted straight lines. This result can be explained by the concentration of charge carriers in the grain boundary which was influenced by the PbO content in the grain boundary. The reason for this behavior was that when PZT ceramics were doped with soft dopants such as lanthanum, the doping ions would occupy A-sites (replacing in Pb^{2+}). When Pb^{2+}, which has smaller ionic radii than La^{3+}, was replaced the extra positive charges (+1)

were introduced into the lattice and a Pb vacancy was created in the lattice to maintain electroneutrality[116]. These Pb vacancies allow an easier transfer of atoms than in a perfect lattice Thus the dielectric constant was higher in comparison to the undoped PZT ceramics.

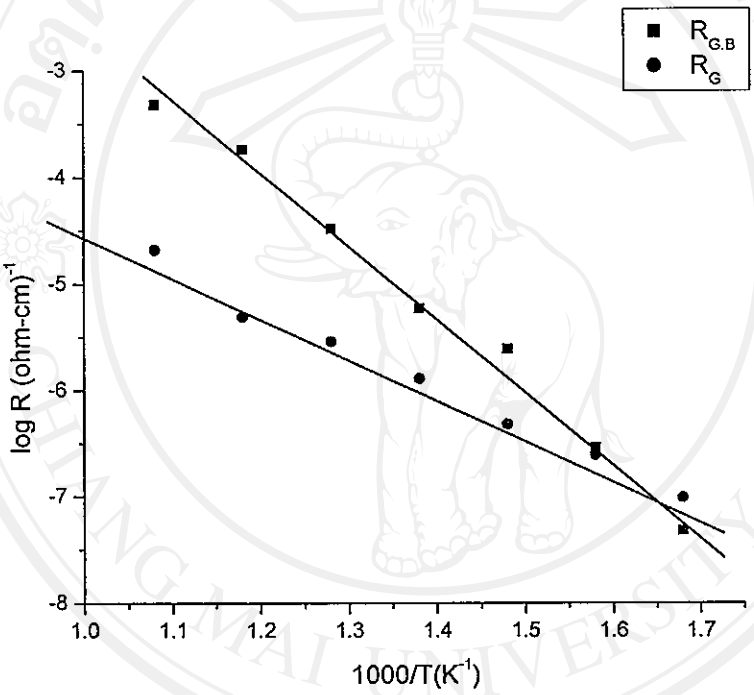

Figrure 3.21 Arrhenius plot for R_G and R_{GB} in PLZT ceramic

3.2.4.2 Ac conductivity of PZT and PLZT

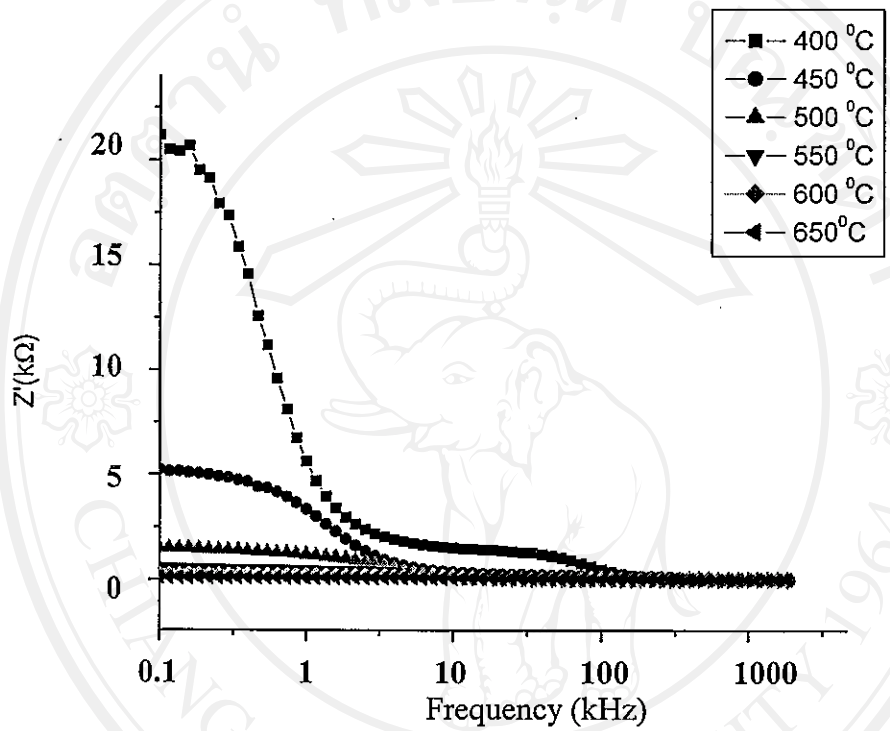

Figure 3.22 The variation of the real part of impedance (Z′) of PLZT ceramic with frequency at different temperatures.

Figure 3.22 shows the variation of the real part of impedance (Z′) with frequency at different temperatures. It can be seen that the curves display a decrease in value of Z′ with frequency at all the temperatures. The magnitude of Z′ decreases with temperatur indicates an increase in the ac conductivity. The Z′ values merge above 150 kHz at all temperature.

The variations of the imaginary part of impedance (Z″) with frequency at different temperatures are shown in Figure 3.23. From the results Z″, values reach a

maxima peak with frequency for temperatures above 500 ^{0}C. For temperatures below 500 ^{0}C, the peak was beyond the range of the frequency measurement. The peaks in Z″ curve shifts to lower frequencies with increasing temperature, indicating the decrease relaxation in the system. The relaxation times were calculated from the frequency at which Z″ maxima were observed. The maximum was found to increase with temperature indicating the increase loss in the sample.

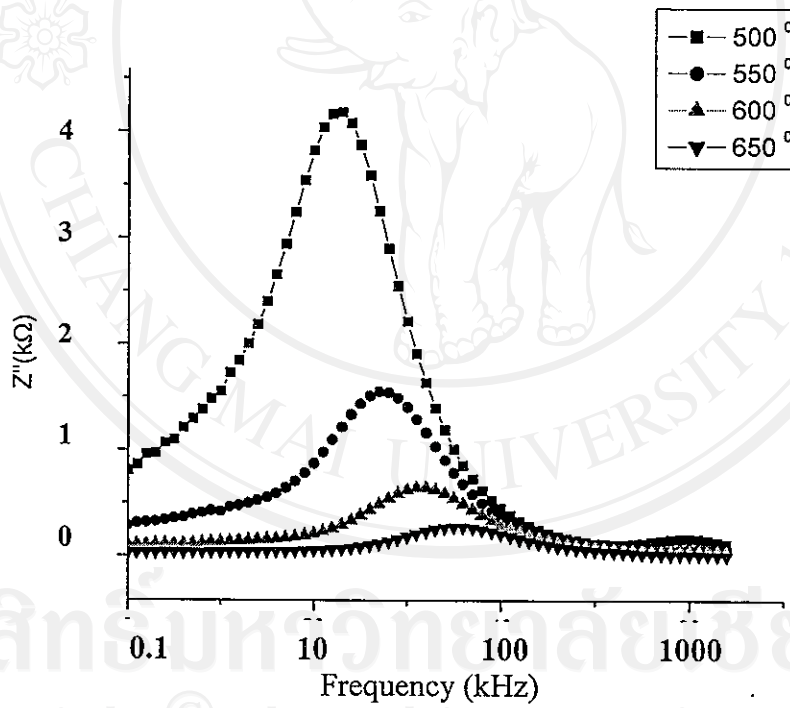

Figure 3.23 The variation of the imaginary part of impedance (Z″) of PLZT ceramics with frequency at different temperatures.

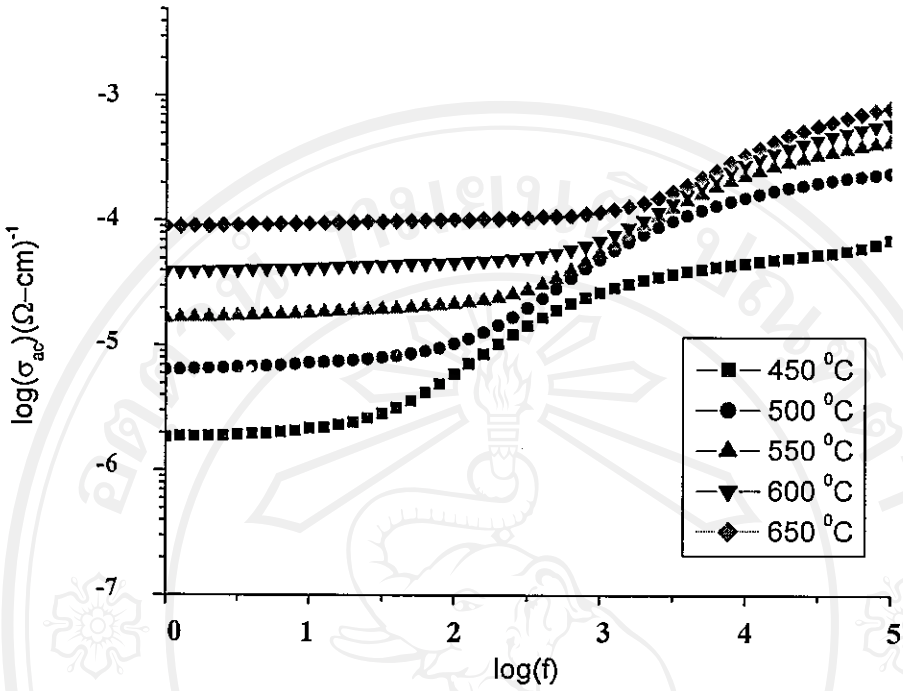

Figure 3.24 The ac conductivity plots of PLZT ceramics as function of frequency at different measured time.

Figure 3.24 shows the a.c conductivity plots of PLZT ceramics as a function of frequency. The frequency dependence of ac conductivity, σ_{ac}, follows a power relation $\sigma_{ac} \alpha \omega^s$, at high frequency. In the low frequency domain a plateau can be observed. In fact, this behavior is show as a further evidence of d.c. conductivity, where conductivity contribution to total-conductivity is independent of the frequency. Thus, the total conductivity can be given by the following equation:

$$\sigma_{tot} = \sigma_{dc} + A\omega^s$$

where σ_{dc} is d.c. conductivity due to excitation of electron from localized states to the conduction bands and $A\omega^s$ is the a.c. conductivity typically assigned to the hopping conduction being while "A" is a frequency independent constant and "s"

is a power with values of $0.0 < s < 1.0$. As a whole, the conductivity behavior is in accordance with conduction mechanism based on the hopping process. Furthermore, a large increase of conductivity in the region between 450 and 650 °C is further evidence of the ac. conductivity as a function of frequency. The hopping conduction frequency is observed to shift to lower frequencies with the increase in temperature. With increasing temperature the charge species that accumulate at grain boundaries have sufficient energy to jump over the barrier, thereby increases the conductivity. Thus the grain boundary resistance decreases beyond this frequency and temperature.

The frequency dependence of the ac conductivity at different temperature for the PZT ceramics is show in Figure 3.25 also corresponding to the power law relation. Consequently, at higher temperature the energy distribution of the energy barriers become more uniform and the variation of the ac conductivity with frequency become less. To understand the above results in terms of the associated activation energy the Arrhenius plots at four selected frequencies of 100 Hz, 1, 10 and 100 kHz are show in figure 3.26. It shows two different activation energies. It can be explained that the activation energy of 0.9 eV in the low temperature region and 1.1 eV in the high temperature region which may be associated with the migration of the oxygen vacancies.

The variation of dielectric constant (ε_r) and dielectric loss (tan δ) with temperature at 1kHz for hydrothermally synthesized PLZT 12/40/60 is shown in Figure 6. The Curie temperature at which the phase transition occurs of 258 ^{0}C is quite high compared to the other reported values of PLZT 12/40/60 ceramics.[4, 22] The PLZT 12/40/60 ceramics synthesized by the nitrate process[4] has the Curie temperature of 140 ^{0}C with dielectric constant of 6,000 while the hot-pressed PLZT 8/40/60 ceramics synthesized by the mixed oxide process[17] has the Curie temperature of 143

^{0}C with dielectric constant of 4435 at the same frequency of 1kHz suggesting that the amount of lanthanum in the hydrothermally synthesized PLZT 12/40/60 ceramics is actually less than 8 at %. The optimum condition to synthesize exactly 12 at % PLZT should be attempted by adding more lanthanum salt, adjusting reaction time, temperature and pH in the final solution before hydrothermal treatment. The dielectric constant of the PLZT ceramics from this study is 1450, which is higher than the value in the PLZT 12/40/60 ceramics synthesized by the mixed oxcide process [22] of the 1270. The dielectric loss of 0.03 is similar as compared to the hot – pressed PLZT 8/40/60 ceramics.[17]

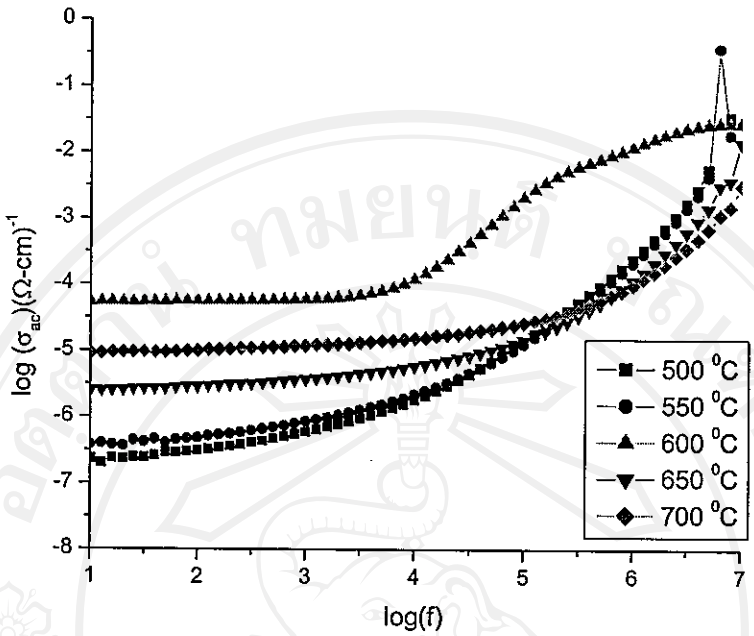

Figure 3.25 The a.c conductivity plots of PZT ceramics as a function of frequency at different measuring time.

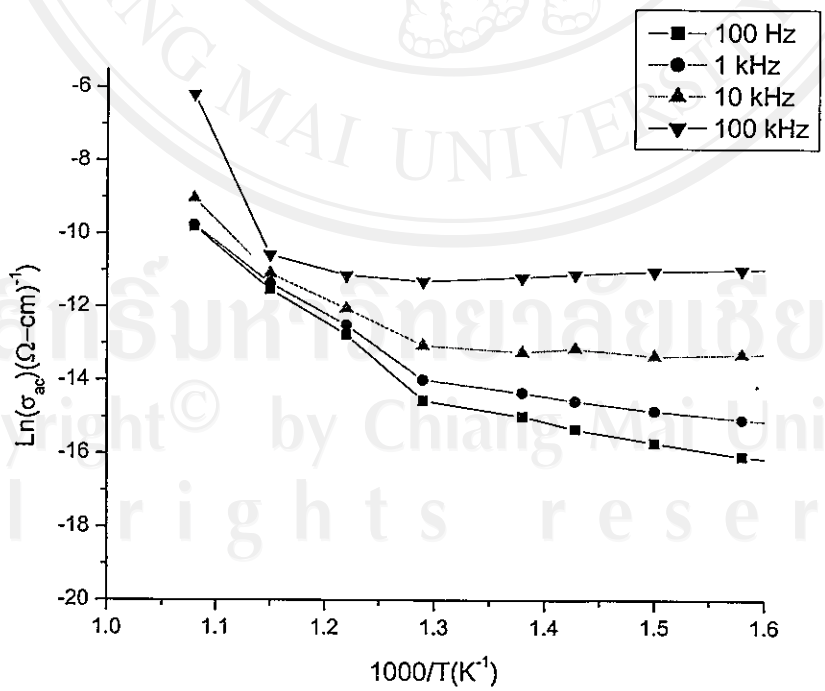

Figure 3.26 Arrhenius plot of PZT ceramic, as a function of frequency at different measuring temperature.

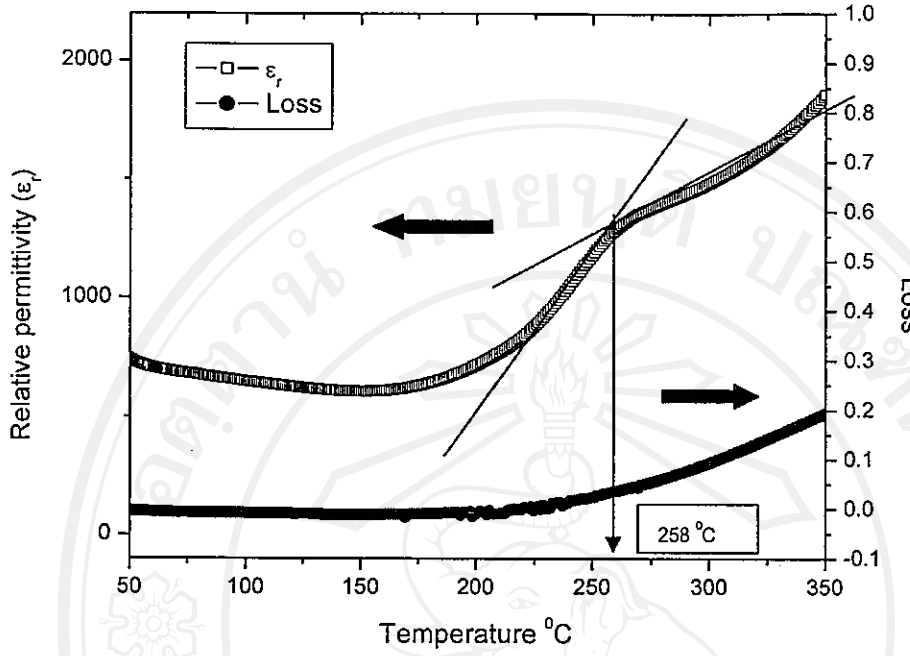

Figure 3.27 Temperature dependence of dielectric constant (ε_r) and dielectric loss (tan δ) for the hydrothermally synthesized PLZT ceramic sintered at 1300 ^{0}C for 3 hours.